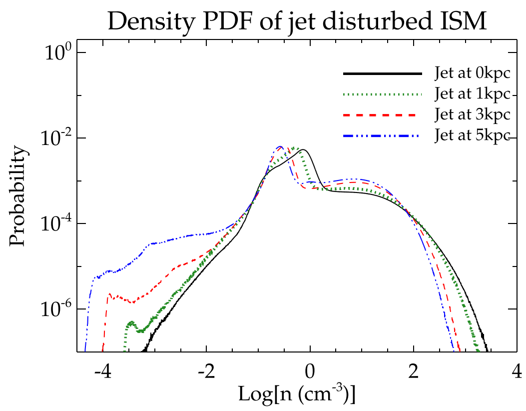

Figure 7. The evolution of the density PDF as the jet evolves with time and breaks out of the dense central region after a height of $z \sim 3$ kpc. The density PDF converges after jet break out as the jet decouples from the ISM.

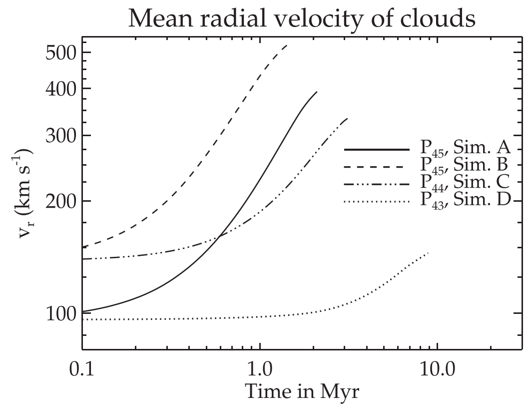

Figure 9. The mass-weighted mean radial velocity ($\int \rho v_r \mathrm{d}^3x / \int \rho \mathrm{d}^3x$) of the warm clouds driven out by the expanding jet-driven bubble.

radially inwards by the backflow near the jet axis. The low-density ablated cloud mass is swept up by the expanding bubble to velocities higher than $\gtrsim$1000 kms^{-1}, flowing out through the channels between the denser clouds (see Fig. 5).

In Figs 10 and 11, we show the evolution of the mean pressure inside the energy bubble and the volume of the bubble. For high-power jets ($P_{\rm jet} \gtrsim 10^{44}$ ergs^{-1}), initially the high-pressure bubble expands nearly adiabatically. The power-law evolution of the pressure in Fig. 10 can be understood by solving the energy equation for an adiabatically expanding bubble, whose volume evolves as in Fig. 11 (see Appendix B for detailed derivation). The evolution of the volume is slower than that of a freely expanding self-similar flow (Castor, McCray & Weaver 1975; Weaver et al. 1977) due to the complex interaction of the bubble with the multiphase ISM. After jet break out, the mean pressure falls more rapidly due to free expansion in the halo. The evolution of the bubble for Sim. D with $P_{\rm jet} = 10^{43}$ ergs^{-1} is much slower compared to the cases with higher $P_{\rm jet}$. The bubble is only weakly overpressured and remains trapped in the ISM for a longer time. This facilitates energy losses via cooling, resulting in slower growth.

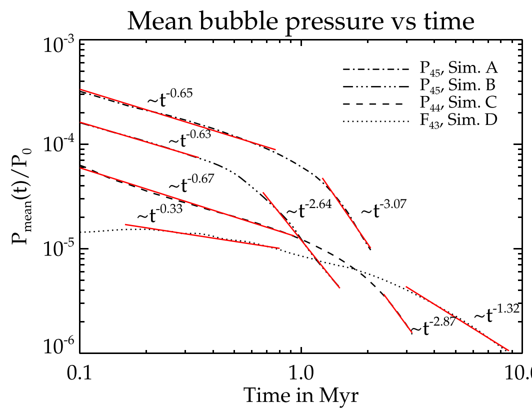

Figure 10. Evolution of the mean pressure inside the energy bubble as a function of time. The red solid lines represent power-law fits to the curves to sections representing before and after the jet break out. The slopes obtained from the fits are noted above the curves.

4.3 Evolution of the phase space

(i) Multiphase ISM:
phase-space diagrams are a useful way to understand the nature of the gas, where different phases of the ISM driven by different

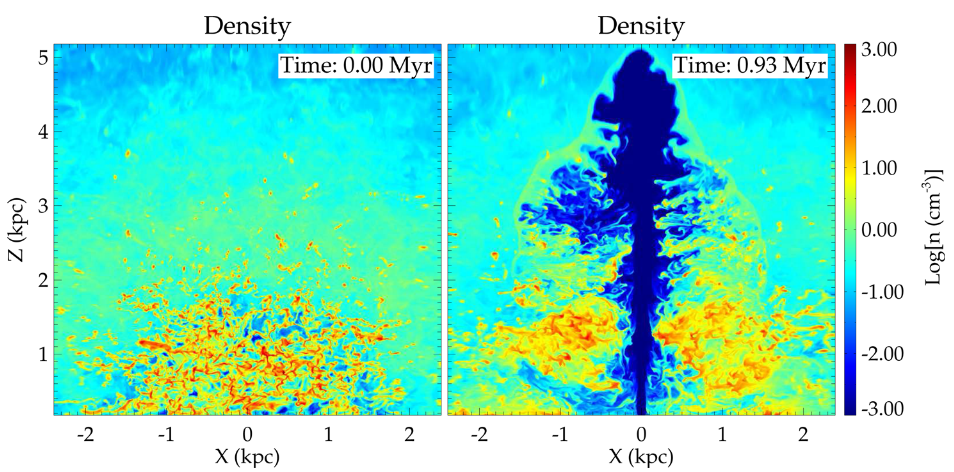

Figure 8. Density ($\log\,[n(\mathrm{cm}^{-3})]$) in the $x - z$ plane for simulation B.

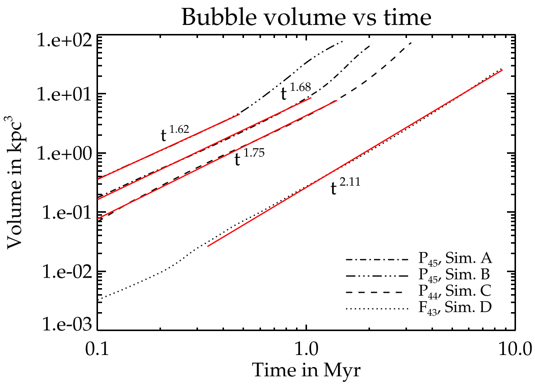

Figure 11. Evolution of the volume of the bubble with time for different simulations. The red solid lines represent power-law fits.

physical mechanisms co-exist. In this section, we discuss the evolution of the phase space of the ISM under the influence of the jet is depicted in Fig. 12. This figure depicts the 2D mass-weighted PDF[3] of p versus ρ and T versus ρ. A mass-weighted PDF gives preferential weights to the dense gas and hence is a more effective probe of the denser ISM than a volume-weighted analysis. Table 4 summarizes the different phases and their labels. At $t = 0$, the simulation domain has a two phase ISM consisting of a low-density HH and a warm dense turbulent filamentary medium (WC) at $T \sim 10^4$ K near the central $\sim$2 kpc (see Fig. 1). Efficient atomic cooling renders the turbulent filaments nearly isothermal as the ISM is allowed to settle prior to the injection of the jet.

With the onset of the jet, two other phases are clearly discernible. At first, a fast-moving forward shock sweeps through the ISM (as shown in Fig. 6) shocking the gas to $\sim 10^5$ K. The ISM shocked by the forward shock is labelled 'FS' in Fig. 12. The forward shock is followed by a slower, nearly adiabatically expanding high-pressure energy bubble with $T \sim 10^6$–10^7 K. (labelled 'EB' in Fig. 12). The energy bubble is nearly homogeneous in pressure and depends only weakly on density as shown by the fits (white dashed lines in Fig. 12) to the mean pressure–density relationship of this phase. At later times, the effective polytropic index of the ISM in the bubble increases slightly as the pressure inside the bubble weakens and the denser filaments start to cool. After the jet has broken out and decoupled from the turbulent ISM ($t \gtrsim 1.33$ Myr, corresponding to the third row of Fig. 12), there still remains a fraction of the gas shocked at $\sim 10^5$ K (RSG). This corresponds to the dense cores of the filaments which having survived shredding by the energy bubble have started to cool.

(ii) Polytropic turbulence:
in Fig. 13, we show the 2D PDF of $\mathcal{M}$ versus ρ, where $\mathcal{M}$ is the mach number defined by $\mathcal{M} = v/c_{\rm s}$, $c_{\rm s}$ being the sound speed. For the settling ISM, the dense filaments form a region of isothermal supersonic turbulence (left-hand panel of Fig. 13). The Mach number is only weakly correlated with the density, similar to previously reported results from numerical simulations of supersonic isothermal turbulence (Kritsuk et al. 2007; Federrath et al. 2010; Federrath & Banerjee 2015). Ideally for isothermal supersonic turbulence, the mach number is independent of the density if the density fluctuations are completely random at all scales (Passot & Vázquez-Semadeni 1998). The weak correlations appearing in the numerical simulations result from strong shocks or rarefactions, where the fundamental assumptions of the independence of the density fluctuations break down (Vazquez-Semadeni 1994; Passot & Vázquez-Semadeni 1998; Federrath et al. 2010). With the onset of the jet, $\mathcal{M}$ and ρ are seen to be positively correlated with density. This is indicative of polytropic turbulence in a medium with polytropic index less than unity (Passot & Vázquez-Semadeni 1998; Federrath & Banerjee 2015), where the PDF deviates from a log-normal distribution.

(iii) Outflow velocity of different phases:
Fig. 14 shows the temperature versus radial velocity ($|v_{\rm r}|$) and density versus radial velocity ($|v_{\rm r}|$) 2D probability density. We see that the passage of the forward shock results in heating up of the ISM to $\sim 10^5$ K as mentioned above without any appreciable increase in radial velocity. The clouds are primarily accelerated by the high-pressure energy bubble to speeds of $\gtrsim 500$ kms^{-1}. In the right-hand panels, we see a tail of very high velocity $\gtrsim 1000$ kms^{-1} with less mass weight. This corresponds to the low-density cloud ablated material swept up by the energy bubble to high radial speeds, as shown in Fig. 5.

5 DEPENDENCE OF MORPHOLOGY ON JET POWER

The coupling of the jet with the ISM depends significantly on the jet power. Jets with higher power, although more efficient in driving powerful outflows, drill through the ISM more rapidly causing less shredding of the cloud cores situated a kiloparsec away from the jet axis. Low-power jets, on the other hand, remain trapped in the ISM for a longer time (see Fig. 15), interacting with the ISM over a much larger volume. In Fig. 16, where we compare the density for jets of different power at a time when the jet head is approximately at the same height for left-hand and right-hand panels. Jets with a power $\sim 10^{45}$ ergs^{-1} evacuate a central cavity of radius $\sim$0.5 kpc, whereas simulation C with $P_{\rm jet} = 10^{44}$ ergs^{-1} a larger cavity ($r \sim 1$ kpc) is evacuated. The situation is more marked for simulation D with $P_{\rm jet} = 10^{43}$ ergs^{-1}, where a larger central cavity is evacuated leaving only a few of the densest cores. The density PDFs of the simulation snapshots in Fig. 16 are presented in Fig. 17. The coefficients of the fits to the high density portion of the density PDF following equation (A7) is presented in Table 5. For simulations with low-power jets, the mean density and dispersion of the density PDF is less than half of their counterparts with $P_{\rm jet} = 10^{45}$ ergs^{-1}. This indicates more shredding of the dense cores by the trapped energy bubble.

The evolution of the phase space is also significantly different for simulation D, as shown in Fig. 18. Unlike the high-power jets, the phase space of the ISM cannot be distinctly divided into a high-pressure energy bubble and gas shocked by the forward shock. The energy bubble is depicted by a horizontal branch in the left-hand panel of Fig. 18. Comparing with the left-hand panel of Fig. 12 depicting the initial condition of the ISM before the jet injection, we find the bubble for Sim. D to be very weakly overpressured. Slow evolution of the bubble facilitates cooling of the shocked gas. Most of the gas swept up by the bubble is shocked to $T \sim 10^5$–10^6 K, lower than that of the high-power jets. The weak bubble is unable to accelerate the clouds to high velocities (as shown in the right-hand panel of Fig. 18). Thus, although the bubble is weak and does not drive significant outflows apparently indicative of weak feedback, its effect on the density distribution is significant, since it is trapped for a longer time inside the ISM.

[3] The mass-weighted PDFs are constructed by evaluating a 2D histogram of a quantity and counting the mass in each simulation cell normalized to the total mass as the weights for a histogram bin.

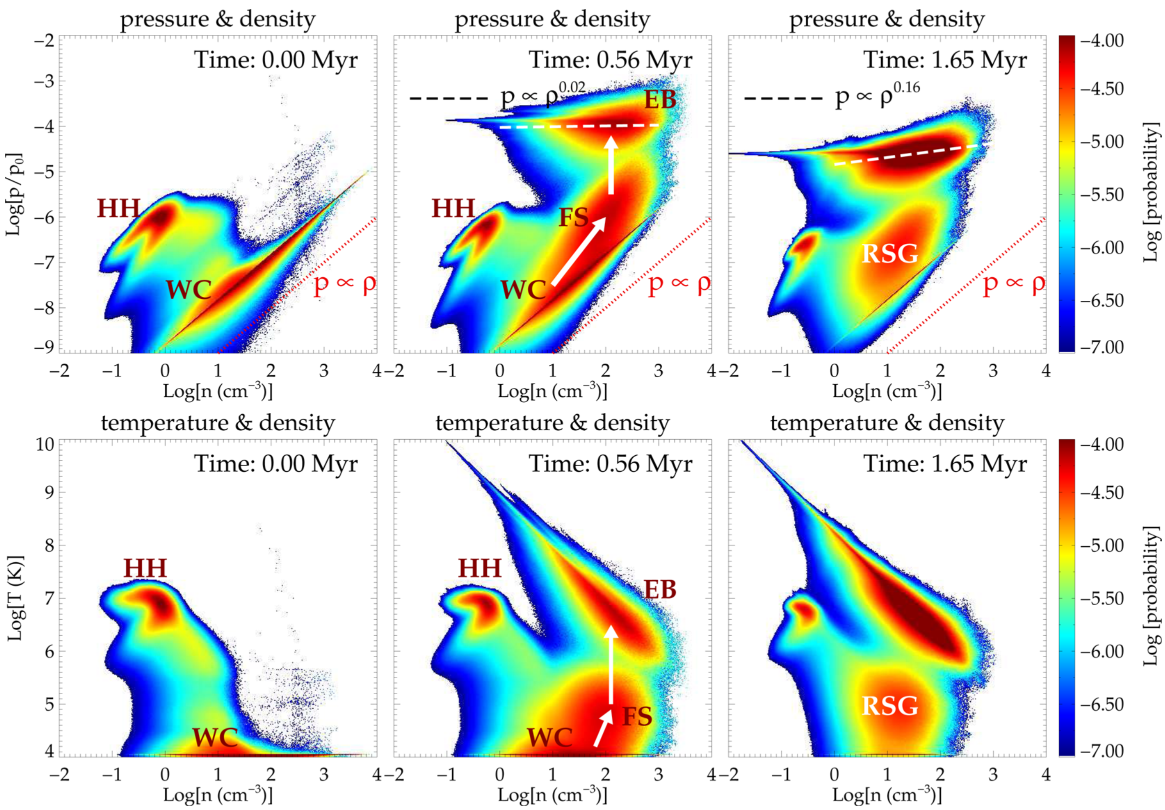

Figure 12. Top: mass-weighted 2D PDF of pressure versus density at times corresponding to plots in Fig. 5. $p_0 = 9.2 \times 10^{-4}$ dynes cm^{-2} is the scale pressure of the simulation. The colour bar denotes the probability. The red dotted line for an isothermal gas is presented to highlight that dense gas closely approximates an isothermal distribution at $t = 0$. The white dashed line represents fits to the mean pressure for the phase corresponding to the energy bubble. The pressure is only weakly related to the density for this phase. Bottom: mass-weighted 2D PDF of temperature versus density. The different ISM phases are labelled as described in Table 4.

Table 4. Summary of different ISM phases.

Phase acronym	Description	Characteristics
HH	Hot Halo	The ambient low-density hot halo. Temperature: $T \sim 10^7$ K.
WC	Warm clouds	Turbulent warm ($T \sim 10^4$K) dense filaments describing the initial ISM.
FS	Forward shock	Shocked ISM behind the initial forward shock. Temperature: $T \sim 10^5$ K. Very little acceleration from initial turbulent velocity.
EB	Energy bubble	High-pressure energy bubble expanding nearly adiabatically for $P_{\rm jet} \gtrsim 10^{44}$ ergs^{-1}. Temperature: $T \sim 10^6$–10^7 K. Accelerates clouds to outward radial velocities $\gtrsim$500 kms^{-1}
RSG	Remnant shocked gas	ISM shocked by the forward shock which remains after jet has decoupled. These represent cooling dense cores of the clouds.

6 ENERGETICS OF THE JET-DISTURBED ISM

6.1 Kinetic energy imparted to the ISM

For any jet power, the jet couples strongly with the ISM initially as it drills through the dense medium. Fig. 19 shows the evolution of the kinetic energy of the dense ISM ($\rho > 1$ cm^{-3}) for different simulations. The kinetic energy rises with time and then decreases after the jet breaks out and decouples from the ISM. For a jet of power $\sim 10^{45}$ ergs^{-1}, the kinetic energy of the ISM increases by a factor of 6 or more, whereas for $P_{\rm jet} \sim 10^{44}$ ergs^{-1} the kinetic energy increases by a factor of 3. The efficiency of jet feedback is better illustrated by plotting the ratio of the kinetic energy of the medium to the total integrated energy input of the jet as a function of time (lower panel in Fig. 19). We see that ∼25–30 per cent of the jet energy is injected into the ISM, for jets of power $\gtrsim 10^{44}$ ergs^{-1}. This is similar to the previous results of (O'Neill et al. (2005), Gaibler et al. (2009), WBU12 and Hardcastle & Krause (2013), where initially the jet is shown to impart ∼20–30 per cent of its energy as kinetic energy to the ISM, while the rest is deposited as internal energy, a fraction of which will be radiated away. More detailed analysis of the energy budget will be presented in a future work.

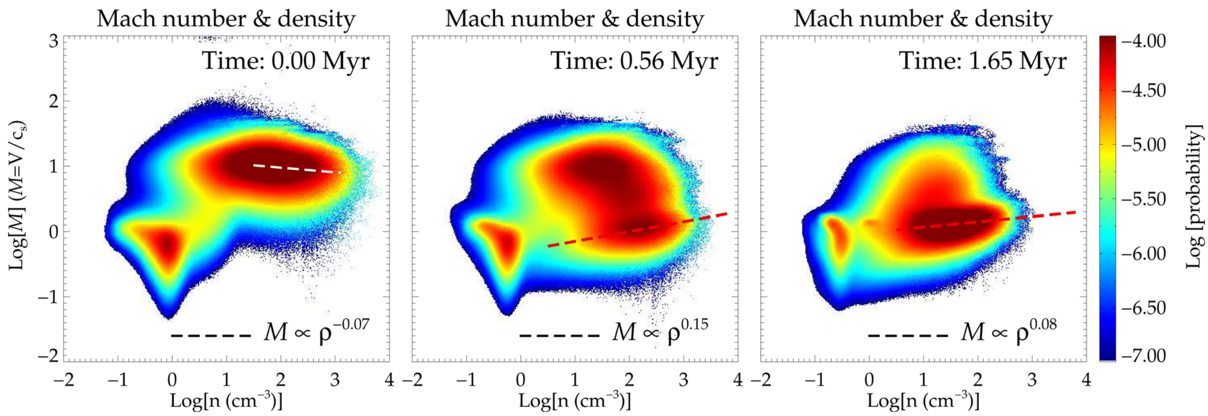

Figure 13. Mass-weighted 2D PDF of log($\mathcal{M}$) versus log (ρ) at times corresponding to plots in Fig. 5. The dashed line represents fits to the mean pressure.

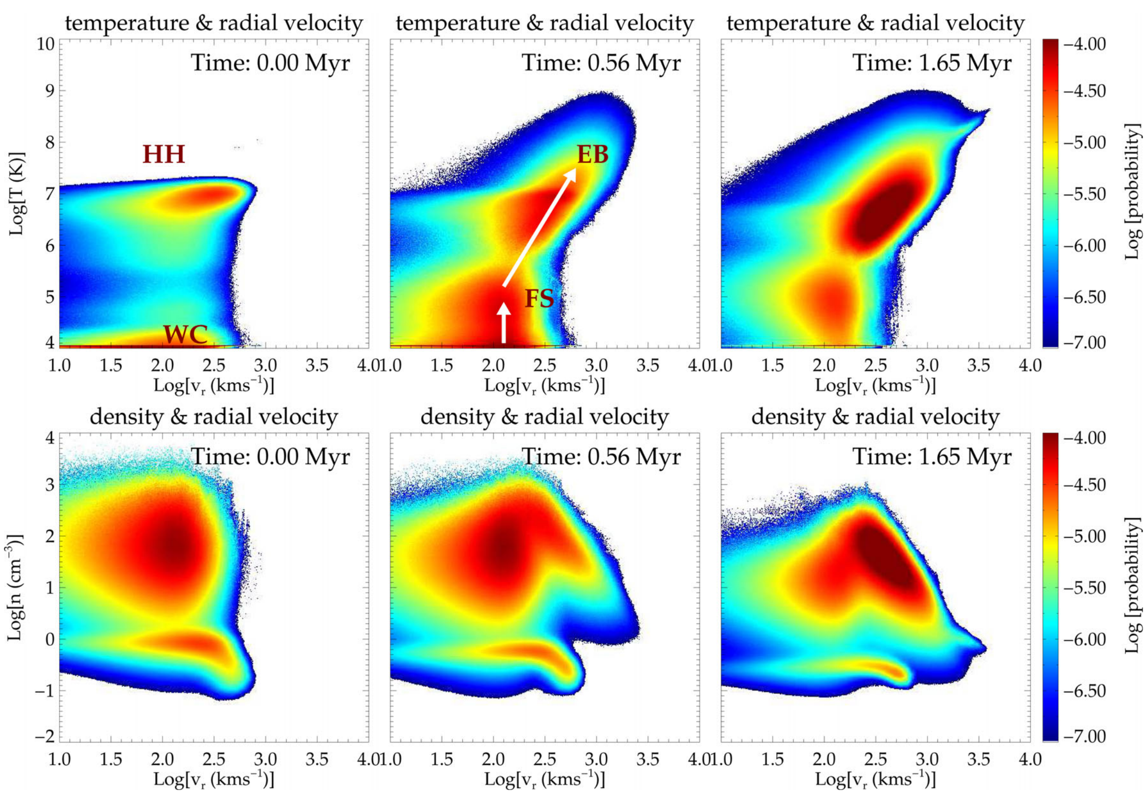

Figure 14. Mass-weighted 2D PDF of temperature versus radial velocity (top) and density versus radial velocity (bottom) at times corresponding to plots in Fig. 5. After the jet injection, the warm dense medium is shocked to $\sim 10^5$ K by the forward shock without an appreciable increase in velocity. Dense gas is accelerated to radial velocities $\gtrsim$500 kms^{-1} by the hot pressure bubble.

The evolution of the kinetic energy is however very different for a low-power jet as in Sim. D with $P_{\rm jet} = 10^{43}$ ergs^{-1}, due to the weakly overpressured nature of the bubble. Although the jet strongly interacts with the ISM in its immediate surroundings, the total kinetic energy of the ISM decreases with time. This is because the jet evolves very slowly and at the initial stages the outer layers of the turbulent ISM are not affected. Even at later stages, since the weakly overpressured bubble evolves very slowly, the bulk kinetic energy of the gas decreases as a result of atomic cooling. Thus, simply computing the ratio of the total kinetic energy of the ISM to the energy injected by the jet as an indicator of the effect of feedback of the jet on the ISM is misleading in this case. The effect of the jet on the density PDF is a better probe of jet-ISM coupling for such cases.

6.2 Galactic fountains and the effect on star formation

Although the high-power jets ($P_{\rm jet} \gtrsim 10^{45}$ ergs^{-1}) launch very fast outflows with speeds $\gtrsim$500 kms^{-1}, the fraction of total mass ejected from the influence of the galaxy's potential is small. In Fig. 20, we show the maximum radial distance the accelerated gas may reach by assuming a ballistic trajectory for the gas and solving $\phi(r_{\rm max}) - \phi(r_0) = v_0^2/2$, for the maximum radius $r_{\rm max}$, where r_0 and v_0 are the initial radius and radial velocity, respectively. In this way, we estimate the fractional mass of the ISM that will reach a given distance. The escape fraction is computed after the jet break out when the jet has decoupled from the ISM and the kinetic energy of the ISM saturates as shown in Fig. 19. We see that only a small fraction of the gas ($\lesssim$5 per cent) goes beyond 10 kpc. Simulation B